ACS OMEGA

http://pubs.acs.org/journal/acsodf

Article

Low-Temperature Synthesis of Disordered Dolomite and High-Magnesium Calcite in Ethanol–Water Solutions: The Solvation Effect and Implications

Yihang Fang, Fangfu Zhang, Gabriela A. Farfan, and Huifang Xu*

Cite This: *ACS Omega* 2022, 7, 281–292

Read Online

ACCESS | Metrics & More | Article Recommendations | Supporting Information

ABSTRACT: How dolomite [$CaMg(CO_3)_2$] forms is still underdetermined, despite over a century of efforts. Challenges to synthesizing dolomite at low temperatures have hindered our understanding of sedimentary dolomite formation. Unlike calcium, magnesium's high affinity toward water results in kinetic barriers from hydration shells that prevent anhydrous Ca–Mg carbonate growth. Previous synthesis studies show that adding low-dielectric-constant materials, such as dioxane, dissolved sulfide, and dissolved silica, can catalyze the formation of disordered dolomite. Also, polar hydrophilic amino acids and polysaccharides, which are very common in biomineralizing organisms, could have a positive role in stimulating Mg-rich carbonate precipitation. Here, we show that disordered dolomite and high-magnesium calcite can be precipitated at room temperature by partially replacing water with ethanol (which has a lower dielectric constant) and bypassing the hydration barrier. Increasing the ethanol volume percentage of ethanol results in higher Mg incorporation into the calcite structure. When the ethanol volume percentage increases to 75 vol %, disordered dolomite (>60 mol % $MgCO_3$) can rapidly precipitate from a solution with [Mg^{2+}] and [Ca^{2+}] mimicking seawater. Thus, our results suggest that the hydration barrier is the critical kinetic inhibitor to primary dolomite precipitation. Ethanol synthesis experiments may provide insights into other materials that share similar properties to promote high-Mg calcite precipitation in sedimentary and biomineral environments.

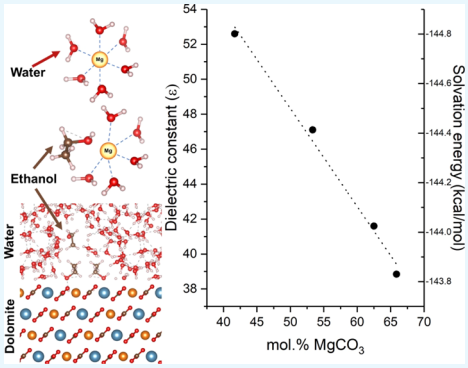

INTRODUCTION

Dolomite [$CaMg(CO_3)_2$] is one of the most abundant carbonates in sedimentary rocks. Although modern seawater is supersaturated with respect to dolomite, contemporaneous precipitation of carbonate in seawater is dominated by aragonite with only rare dolomite occurrences. This creates a discrepancy with observations in the geologic record where massive sedimentary dolomite deposits have been found. This contradiction in dolomite prevalence combined with difficulties in synthesizing dolomite or its precursor phases (high Mg-calcite, protodolomite, and disordered dolomite) at room temperature in the past defines the long-standing "dolomite problem".[1−6] In modern settings, primary dolomite is mainly reported in extreme or uncommon environments such as alkaline lakes,[7−9] deep marine carbonate pavements associated with methane seeps,[10−13] and shallow marine environments with microbial mats.[14−17]

Low-temperature synthesis of dolomite has been unsuccessful for decades, even with oversaturated solutions and prolonged experiments.[4] Although dolomite has been recognized as thermodynamically stable in modern seawater,[18−20] low-temperature synthesis attempts of dolomite close to seawater composition have only produced aragonite and calcite. One of the main issues in synthesizing dolomite in aqueous solutions is magnesium's strong affinity for water with higher enthalpy[21−23] and slower exchange rate[24] compared to other divalent ions. Water molecules strongly bond with free Mg^{2+} in solution and inhibit Mg^{2+} from incorporating into the crystal[21,25−28] or it bonds with crystal-surface Mg^{2+}, preventing Mg^{2+} from bonding with CO_3^{2-} and hindering the crystal growth.[29] Consequently, magnesium usually incorporates into hydrate mineral phases, such as nesquehonite ($MgCO_3 \cdot 3H_2O$), lansfordite ($MgCO_3 \cdot 5H_2O$), hydromagnesite [$Mg_5(CO_3)_4(OH)_2 \cdot 4H_2O$], and dypingite [$Mg_5(CO_3)_4(OH)_2 \cdot 5H_2O$] in a Mg-bearing solution at room temperature.[30,31] Therefore, the dehydration of the Mg–water complex is considered the most critical barrier for dolomite nucleation and growth.[21,27,32]

Many successful attempts at low-temperature disordered dolomite precipitation have been demonstrated in the past years with the presence of catalysts.[33−38] These catalysts,

Received: August 24, 2021
Accepted: December 3, 2021
Published: December 17, 2021

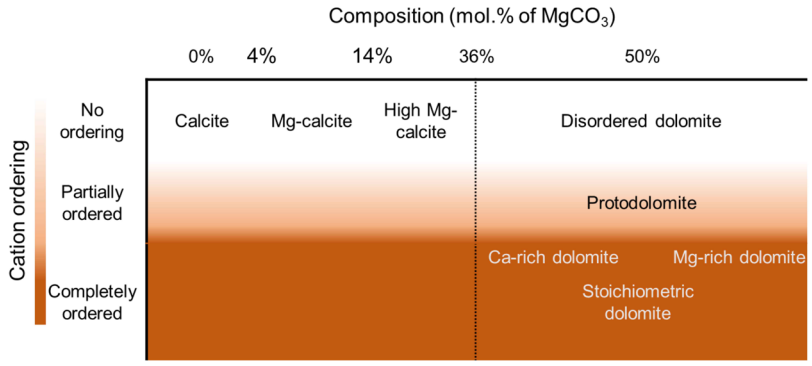

Figure 1. Ca−Mg carbonate terminology used in this work. The classification of disordered dolomite, protodolomite, and HMC is based on previous works.[45,46] The color scale on the left side indicates cation ordering states.

Table 1. Different Ethanol Percentage Conditions for the Ethanol−Water Mixture to Precipitate Ca−Mg Carbonates[a]

	solution conditions										
sample #	ethanol vol %	temp (°C)	$[Mg^{2+}]$ (mM)	$[Ca^{2+}]$ (mM)	$[HCO_3^-]$ (mM)	seeds	initial pH	final pH	Mg/Ca	mineral phases present	$MgCO_3$ content
S53	30	25	50 ± 0.1	10 ± 0.1	50 ± 0.1	N	7.6	8.4	5:1	Hmc, Hmg	21.6 ± 1
S54	50		50 ± 0.1	10 ± 0.1	50 ± 0.1	N	7.7	8.7	5:1	Dol, Arg*	46.6 ± 2
S55	75		50 ± 0.1	10 ± 0.1	50 ± 0.1	N	7.7	8.8	5:1	Dol, Arg	44.1 ± 2
S5	50	50	50 ± 0.1	10 ± 0.1	50 ± 0.1	N	7.5	8.7	5:1	Dol, Arg, Hmg	51.0 ± 2
S15	60		50 ± 0.1	10 ± 0.1	50 ± 0.1	N	7.5	8.7	5:1	Dol, Arg, Hmg	51.7 ± 2
S25	70		50 ± 0.1	10 ± 0.1	50 ± 0.1	N	7.5	8.7	5:1	Dol, Hmg, Arg*	56.6 ± 2
S35	75		50 ± 0.1	10 ± 0.1	50 ± 0.1	N	7.4	8.6	5:1	Dol, Cal, Arg	57.2 ± 2
S10	50	50	100 ± 0.1	10 ± 0.1	50 ± 0.1	N	7.4	8.6	10:1	Dol, Hmg	55.3 ± 2
S20	60		100 ± 0.1	10 ± 0.1	50 ± 0.1	N	7.4	8.6	10:1	Dol, Arg, Hmg*	50.4 ± 2
S30	70		100 ± 0.1	10 ± 0.1	50 ± 0.1	N	7.4	8.6	10:1	Dol, Arg, Hmg*	54.1 ± 2
S40	75		100 ± 0.1	10 ± 0.1	50 ± 0.1	N	7.4	8.6	10:1	Dol, Cal, Arg, Hmg	53.5 ± 2
S48	75	25	50 ± 0.1	10 ± 0.1	50 ± 0.1	Y	7.7	8.5	5:1	Dol, Arg, Hmg*	48.0 ± 2
S52	75	50	50 ± 0.1	10 ± 0.1	50 ± 0.1	Y	7.5	8.3	5:1	Dol, Arg, Cal*	51.0 ± 2
control 1	0	25	50 ± 0.1	10 ± 0.1	50 ± 0.1	N	7.7	8.5	5:1	Arg, Cal*	2.1 ± 1
control 2	0	50	50 ± 0.1	10 ± 0.1	50 ± 0.1	N	7.5	8.4	5:1	Arg, Cal *	-
control 3	0	25	100 ± 0.1	10 ± 0.1	50 ± 0.1	N	7.6	8.4	10:1	Arg, Mg-Cal*	6.1 ± 1
control 4	0	50	100 ± 0.1	10 ± 0.1	50 ± 0.1	N	7.4	8.2	10:1	Arg, Mg-Cal*	6.3 ± 1
control 5	0	25	50 ± 0.1	10 ± 0.1	50 ± 0.1	Y	7.6	8.5	10:1	Arg, Cal*	2.1 ± 1
control 6	0	50	50 ± 0.1	10 ± 0.1	50 ± 0.1	Y	7.5	8.4	10:1	Arg, Mg-Cal*	7.3 ± 1

[a]Dol = Disordered dolomite, Cal = calcite, Mg-Cal = Mg-calcite, Arg = aragonite, Hmc = high-magnesium calcite, and Hmg = hydromagnesite. * = trace amount.

including dioxane, polysaccharides, exopolymeric substances (EPSs), and aqueous $Si(OH)_4$, either have low dipole moments (silica and dioxane) or have −OH groups that will form a hydrogen bond with CO_3^{2-} on carbonate surfaces (polysaccharide and EPS). We recognize that the hydration problem is not the only limiting factor in inhibiting dolomite growth in a low-temperature environment. Other factors are lattice limitation,[32] difference in cation properties,[39] and reduced surface energy from cation disordering.[40] However, the hydration barrier is a first step to consider prior to Mg^{2+} incorporation into the calcite structure and CO_3^{2-} bonding with surface Mg^{2+} during (disordered) dolomite precipitation. Many previous works have investigated the effects of ethanol−water mixtures on the precipitation of calcite in Mg-free solutions to demonstrate that different ethanol concentrations could change the polymorph of $CaCO_3$ to calcite, aragonite, or vaterite.[41,42] Seo et al.[41] suggested that increasing ethanol volume percent over 50 vol % leads to preferential precipitation of aragonite and vaterite, whereas lower ethanol volume percent experiments are dominated by calcite structures. Sand et al.[42] also demonstrated a similar effect: with increasing ethanol or propanol in solution, the amount of aragonite also increases. Yet, few attempts have been made to synthesize carbonates in a water−alcohol mixture with magnesium. Liu et al.,[43] using 10× seawater Mg and Ca concentrations, observed that lower ethanol concentrations (≤33 vol %) result in a mixture of aragonite and calcite, while higher ethanol concentrations are dominated by pure aragonite. On the other hand, Falini et al.[44] revealed Mg-calcite with up to ∼14 mol. $MgCO_3$ can be precipitated in different water−alcohol mixtures, that is, methanol, ethanol, and propanol. Therefore, this study is designed to bypass the hydration barrier of Mg^{2+} cations, test the validity of water inhibition on dolomite formation, and investigate other factors that impact dolomite nucleation.

METHODS

Carbonate Terminology. To identify and characterize the dolomite and dolomite precursor phases in our experiments, we follow these definitions: Gregg et al.[45] describe high-

https://doi.org/10.1021/acsomega.1c04624
ACS Omega 2022, 7, 281−292

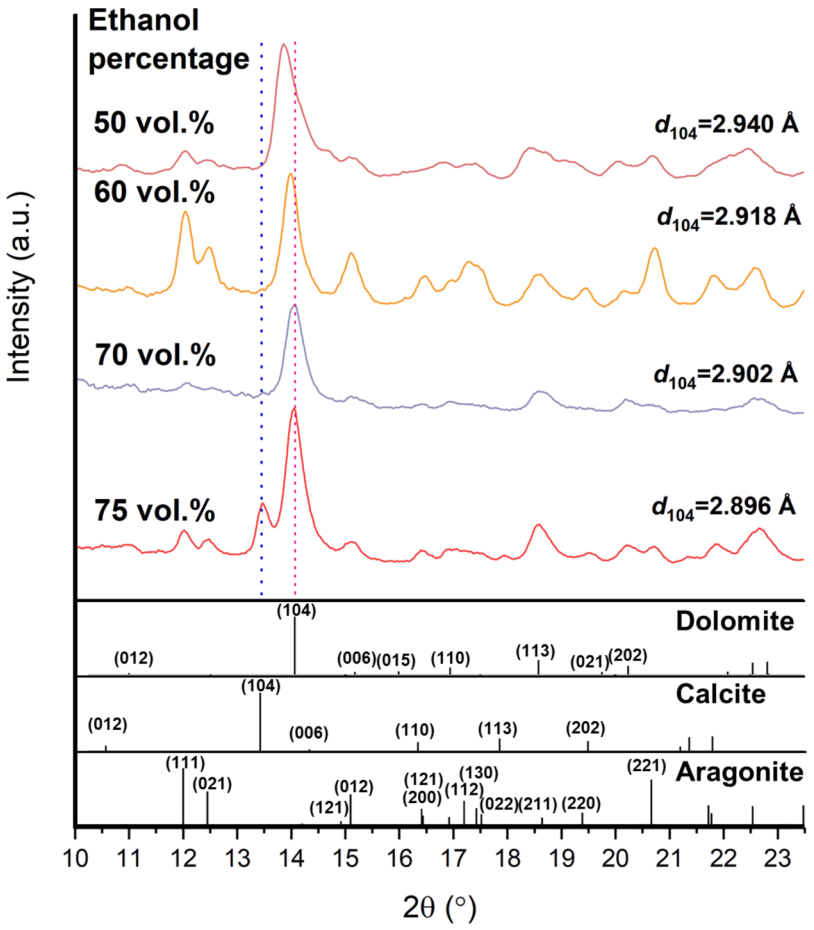

Figure 2. XRD patterns (Mo K-alpha radiation) of typical samples from solutions without calcite seeds in different volume percentages of ethanol at 50 °C and 50 mM [Mg^{2+}]. A systematic shift in the disordered dolomite (104) peak toward a higher angle as a function of higher ethanol percentages reflects decreasing unit cell parameters due to the increased incorporation of magnesium in these carbonates. 50 vol % = S5, 60 vol % = S15, 70 vol % = S25, and 75 vol % = S35. Blue dashed line = calcite reference (104) peak position. Red dashed line = stoichiometric dolomite reference (104) peak position. Bottom are dolomite, calcite, and aragonite reference peaks.

magnesium calcite (HMC) as a compound containing 4−36 mol % $MgCO_3$, Fang and Xu[46] describe disordered dolomite as >36 mol % $MgCO_3$ with no cation ordering, and protodolomite as >36 mol % $MgCO_3$ with the evidence of partial cation ordering (Figure 1). Disordered dolomite and HMC are considered to be precursor phases for sedimentary dolomite, where both phases have no cation ordering and $R\bar{3}c$ symmetry, compared to $R\bar{3}$ for stoichiometric dolomite.[5,35,45,47] The reduced symmetry of stoichiometric dolomite results in an extra set of reflections or "*b*"-reflections, such as (10$\bar{5}$), (101), and (003).

Synthesis Experiments. We conducted closed-system free-drift synthesis experiments in sealed polyethylene bottles. Experiments testing the impact of ethanol content and temperature on dolomite precipitation were conducted at 50−75 vol % ethanol and at 25, 40, and 50 °C (outlined in Table 1). 50 or 100 mM $MgCl_2{\cdot}6H_2O$ was added to 10 mM $CaCl_2{\cdot}H_2O$ and 50 mM $NaHCO_3$ (Fisher Chemical) with distilled deionized (DI) water. After constantly mixing for 30 min, solutions were divided into either 5 or 10 50 mL sized bottles and kept in a Thermo Scientific Heratherm General Protocol oven for time series analysis (24−289 h). Calcite-seeded solutions followed protocols established by previous studies with 1 g/L of calcite seeds, which have a surface area per calcite seed mass of 9.8 m^2/g.[38] Solutions were then filtered with filter papers (GE Whatman, 20−25 μm pore size) and air-dried for X-ray diffraction (XRD), energy-dispersive spectrometry (EDS), and transmission electron microscopy (TEM) analyses. Saturation indices for different phases were calculated using the PHREEQC geochemical program.[48]

Analytical Procedures. Filtered and dried powders were filled into Kapton or glass tubes with a 1 mm inner diameter for power XRD analysis using a Rigaku Rapid II XRD system (Mo Kα radiation, λ = 0.7093 Å). Diffraction patterns were collected by a 2-D image-plate detector, and patterns were converted into traditional 2θ versus intensity using Rigaku 2DP software. Mineral phases were identified using the MDI Jade 9.5 software package with the American Mineralogist Crystal Database (AMCSD) and the PDF-4+ database from the International Centre for Diffraction Data (ICDD). Rietveld refinements for unit cell parameters, crystal sizes, phase fractions, and crystallinity were done using the Bruker TOPAS program and crystal structures from the AMCSD. Pearson VII peak functions were used for all refinements. We used the d_{104} values of calcite and dolomite structures to estimate $MgCO_3$ percentages in Ca−Mg carbonates based on an empirical curve.[46,49]

Scanning electron microscopy (SEM) and EDS were performed using a Hitachi S3400 instrument at the Geoscience Department of University of Wisconsin−Madison. EDS results

https://doi.org/10.1021/acsomega.1c04624
ACS Omega 2022, 7, 281−292

Table 2. Solution Conditions for the Ethanol−Water Mixture with Different Alkalinities to Precipitate Ca−Mg Carbonates[e]

sample #	volume ratio[a]	Mg/Ca ratio	T (°C)	calcite seeds	mineral phases present	d_{104} (Å) of Ca−Mg carbonates	$MgCO_3$ content based on XRD (mol %)[b]
S56	3:3	5:1	25	N	Dol, Arg	2.9529	41.1 ± 2
S57	3:4	5:1	25	N	Dol, Arg	2.9451	43.5 ± 2
S58	3:5	5:1	25	N	Dol, Arg, Mhc	2.9367	46.1 ± 2
S59	3:4	5:1	25	Y	Dol, Cal, Arg*	2.9326	47.4 ± 2
S60	3:5	5:1	25	Y	Dol, Cal	2.9241	49.9 ± 2
S61	3:6	5:1	25	Y	Dol, Cal	2.9157	52.5 ± 2
S62	3:4	5:1	50	Y	Dol, Cal	2.8871	60.8 ± 2
S63	3:5	5:1	50	Y	Dol, Cal	2.8830	62.0 ± 2
S64	3:6	5:1	50	Y	Dol, Cal	2.8750	64.3 ± 2
S65	3:4	10:1	25	N	Dol	2.9307	47.9 ± 2
S66	3:5	10:1	25	N	Dol	2.9280	48.8 ± 2
S67	3:4	10:1	25	Y	Dol, Cal, Arg*	2.9282	48.7 ± 2
S68	3:5	10:1	25	Y	Dol, Cal	2.9158	52.4 ± 2
S69	3:6	10:1	25	Y	Dol, Cal	2.9111	53.8 ± 2
S70	3:4	10:1	50	Y	Dol, Cal	2.8792	63.1 ± 2
S71	3:5	10:1	50	Y	Dol, Cal	2.8711	65.4 ± 2
							66.6 ± 2
S72	3:6	10:1	50	Y	Dol, Cal	2.8667	69.6%[c] (64.4% ∼ 74.2%)[d]

[a]Volume ratio of $MgCl_2$ + $CaCl_2$ + ethanol solution to $NaHCO_3$ + ethanol solution. [b]Molar content of $MgCO_3$ based on the Zhang et al. (2010) and Fang and Xu (2019) curve. [c]Average $MgCO_3$ content based on TEM EDS data. [d]$MgCO_3$ content variation based on TEM EDS data. [e]Dol = Disordered dolomite, Cal = Calcite, Arg = aragonite, Mhc = monohydrocalcite, and * = trace amount.

were calibrated using a dolomite standard (Delight dolomite) with 50.48 mol % $MgCO_3$.[34,38,46] Samples were coated using 10 nm thick carbon. TEM measurements were carried out using a Philips CM200UT TEM instrument operating at 200 kV acceleration voltage with a 0.5 mm spherical aberration (Cs) and a point resolution of 0.19 nm in the Material Science and Engineering Department at the University of Wisconsin−Madison.

RESULTS

Ethanol−Water Mixtures without Calcite Seeds. Solutions changed from transparent to opaque in all experiments within 20 min after mixing, indicating rapid precipitation. Significant increases in pH, from 7.4−7.7 to 8.3−8.7, were observed in all experiments, presumably from the precipitation of carbonates equilibrating with CO_2 in the bottle headspace (Table 1). XRD patterns of synthesis experiments confirmed that ethanol can induce precipitation of HMC and disordered dolomite (Figure 2 and Table 2). XRD patterns of typical samples displayed no obvious ordering reflection, or "*b*"-reflection, in the synthesized samples which would indicate the presence of an ordered dolomite phase. The systematic shifts of peaks in the XRD patterns toward higher angles resulted from decreasing lattice parameters of the precipitated Ca−Mg carbonate from increasing Mg incorporation (Figure 2). With an initial Mg/Ca ratio of 5:1 solution with 50 vol % ethanol and no calcite seeds at 50 °C, the d_{104} value of disordered dolomite was 2.9395 Å, corresponding to 45.3 mol % $MgCO_3$ based on the empirical curve for disordered dolomite.[46,49] On the other hand, control experiments containing no ethanol only produced HMC with 2−6 mol % of $MgCO_3$ (Table 1). With the increasing ethanol percentage, the $MgCO_3$ content in disordered dolomite increased from 45.3 mol.% to 51.7, 56.6, and 57.2 mol % $MgCO_3$ precipitated from solutions with 50, 60, and 70 vol.% to 75 vol % ethanol with 50 mM [Mg^{2+}] at 50 °C, respectively (Figure 2 and Table 2). However, the Mg percentage in carbonate precipitates from ethanol solutions with 100 mM [Mg^{2+}] appeared to be independent to increasing ethanol concentrations, with mol % $MgCO_3$ ranging from 50.39 to 55.31 mol % (Table 2).

Moreover, the $MgCO_3$ content in precipitates consistently shifted toward higher values with increasing temperature (25 vs 50 °C) for precipitates formed with 50 vol % ethanol and 50 mM [Mg^{2+}] (Table 2). The temperature effect is even more pronounced in the precipitates from higher-ethanol-percentage solutions (Table 1).

Ethanol−Water Mixtures with Calcite Seeds. The seeded effect, where seed crystals provide a crystal template allowing for faster crystal growth, is clear in all seeded synthesis experiments. Experiments with calcite seeds showed decreasing mol % $MgCO_3$ with increasing ethanol percentage (Figure 3). For example, precipitates from 50 vol % ethanol with 50 mM [Mg^{2+}] at 25 °C had a 53.7−54.8 mol % $MgCO_3$ compared to 50.7−52.4 mol % $MgCO_3$ from 75 vol % ethanol with 50 mM [Mg^{2+}] (Figure 4). This trend is also observed at 50 °C, such that carbonates precipitated at 50 vol % ethanol with 50 mM [Mg^{2+}] have 64.3−66.6 mol % $MgCO_3$ content versus 53.8 mol % $MgCO_3$ content from solution with 75 vol % ethanol with 50 mM [Mg^{2+}] (Figure 5).

The $MgCO_3$ content in seeded experiments was significantly higher compared to that in seedless experiments (Figures 4 and 5 and Tables 1 and 2). This effect is most pronounced in the 50 mM Mg solutions. For example, precipitates from seeded experiments with a 5:1 Mg/Ca ratio, 25 °C, and 50 vol % ethanol have 47.4−49.9 mol % $MgCO_3$ compared to 43.5−46.1 mol % $MgCO_3$ in parallel unseeded experiments. The differences in Mg incorporation between seedless and seeded experiments diminish at 50 °C, compared to those at 25 °C.

In contrast to our seedless ethanol experiments, the dominant product in our ethanol-free control experiments was aragonite rather than Mg-rich calcium carbonates (Table 2). Aragonite is absent in all calcite-seeded experiments with ethanol. In calcite-seeded experiments, aragonite is absent with

https://doi.org/10.1021/acsomega.1c04624
ACS Omega 2022, 7, 281−292

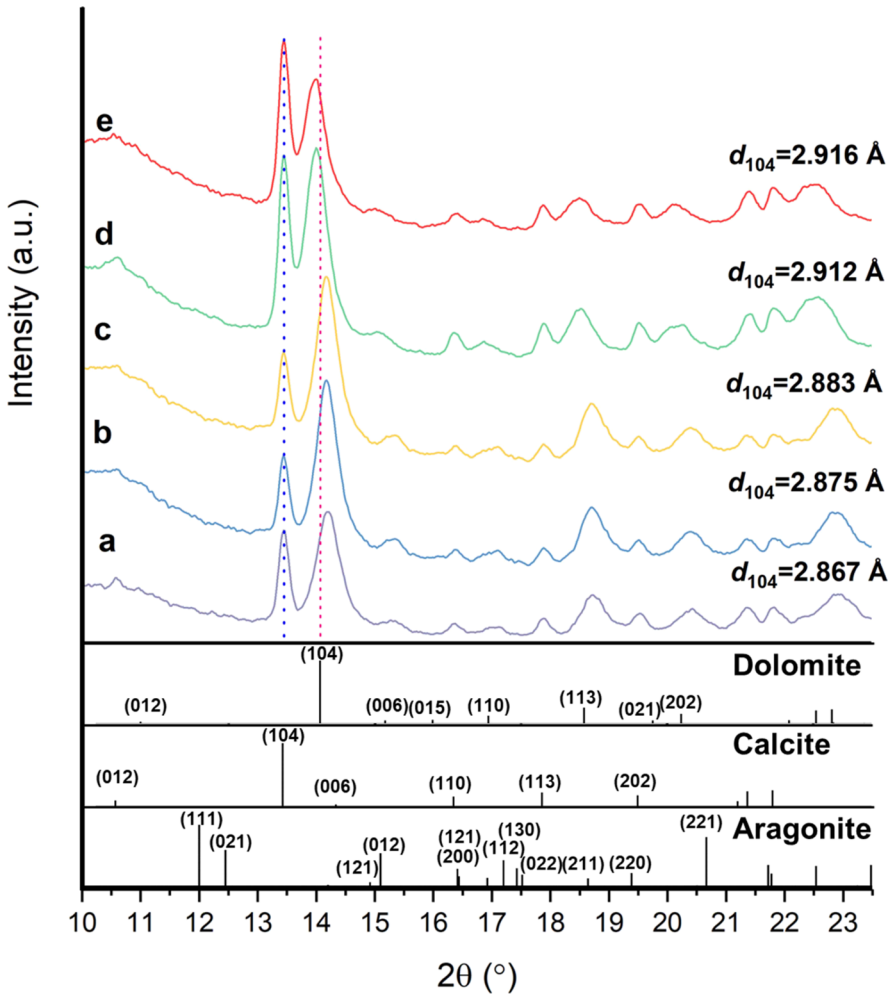

Figure 3. XRD patterns of typical samples from solutions with calcite seeds under different conditions. Experiments performed at (a) 50 °C and 100 mM [Mg^{2+}] with 50 vol % ethanol; (b) 50 °C and 50 mM [Mg^{2+}] with 50 vol % ethanol; (c) 75 °C and 50 mM [Mg^{2+}] with 75 vol % ethanol; (d) 25 °C and 100 mM [Mg^{2+}] with 50 vol % ethanol; and (e) 25 °C and 50 mM [Mg^{2+}] with 50 vol % ethanol. a = S72, b = S64, c = S63, d = S69, and e = S61. Blue dashed line = calcite reference (104) peak position. Red dashed line = stoichiometric dolomite reference (104) peak position. Bottom are dolomite, calcite, and aragonite reference peaks.

only calcite in the ethanol-free controls. In all synthesized samples, diffraction patterns show humps at low angles, indicating the presence of nanosized particles. No obvious amorphous calcium carbonate (ACC) and amorphous calcium magnesium carbonate (ACMC) have been observed in XRD patterns around 3.1 Å based on the results from Xu et al. The seeded experiments consistently show a lower final pH than the seedless experiments under the same conditions.

Other than disordered dolomite and HMC, two metastable phases nesquehonite [$Mg(HCO_3)(OH)\cdot H_2O$] and hydromagnesite [$Mg_5(CO_3)_4(OH)_2\cdot 4H_2O$] may also form. Nesquehonite and hydromagnesite are found in all 50 °C experiments but only in several cases at 25 °C. At 50 °C, nesquehonite will dehydrate and transform into hydromagnesite after ∼60 h. A recent study has shown that solution with a high concentration of Ca, Mg, and carbonate and high pH can result in the formation of ACMC which later transforms into nesquehonite, monohydrocalcite, and disordered dolomite.[50] The cause of the dehydration of these hydrate Mg-carbonate phases is not clear and is beyond the purpose of this study.

Scanning Electron Microscopy. SEM images showed that spherulite-shaped disordered dolomite overgrew Mg-calcite in ethanol solutions with no calcite seeds (Figure 6A). However, disordered dolomite that precipitated from ethanol solutions with calcite seeds grew into irregular shapes, indicating that calcite seeds likely provide heterogeneous nucleation sites for Mg-bearing carbonate growth (Figure 6B).

Transmission Electron Microscopy. TEM analyses showed that disordered dolomite overgrew and surrounded calcite in seeded experiments (Figure 7). TEM also revealed that dolomite formed in ethanol solutions as nanocrystals (∼10 nm) with well-developed crystal {104} faces (Figure 7). We note that these nanocrystals were not randomly oriented but followed a similar orientation with low-angle boundaries (Figure 7C). Low-angle boundaries were also observed in selected-area electron diffraction (SAED) as diffraction arcs of about ∼10°, instead of distinctive spots seen from a single-crystal region or complete rings as seen from random crystal orientations (Figure 7D). The absence of super-lattice "*b*"-reflections [e.g., ($10\bar{5}$), (101), and (003)] in both SAED and fast Fourier transform from high-resolution TEM (HRTEM) images indicates that these precipitated Ca−Mg carbonates have a calcite structure with a completed disordered cation or $s^* = 0$ following the notation for the cation ordering state from Fang and Xu.[46]

https://doi.org/10.1021/acsomega.1c04624
ACS Omega 2022, 7, 281−292

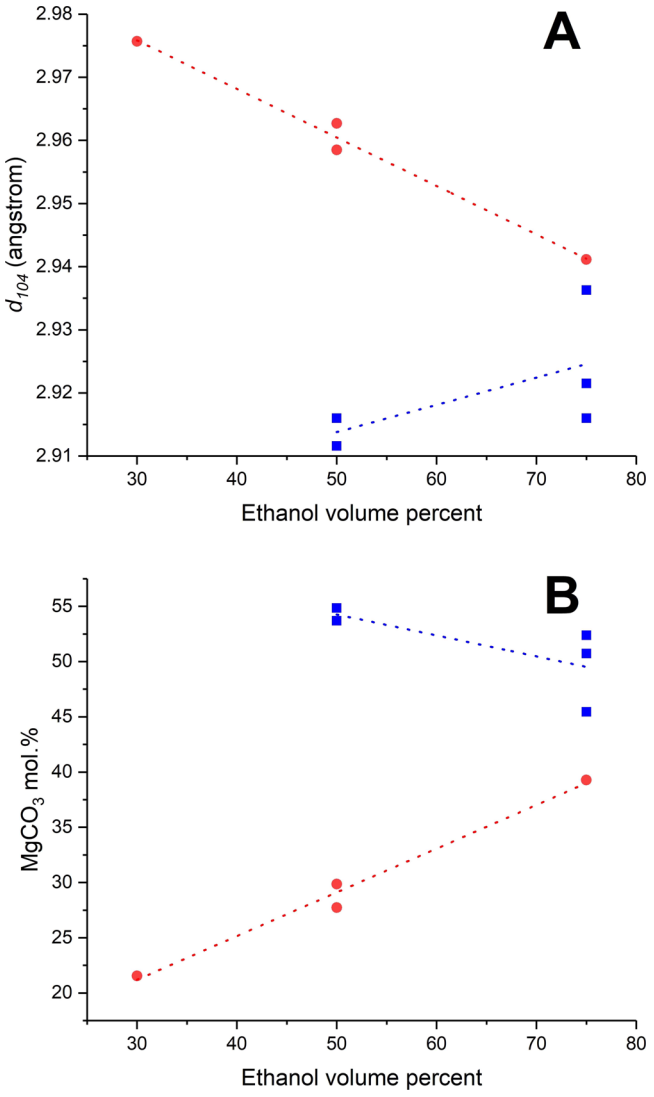

Figure 4. XRD Rietveld refinement results for experiments with 50 mM [Mg^{2+}] at 25 °C as (A) d_{104} values and (B) $MgCO_3$ mol % as a function of ethanol vol %. Red circles correspond to seedless experiments, and blue squares correspond to seeded experiments. Errors associated with the *y*-axes are ±0.004 Å (A) and ±2 mol % (B).

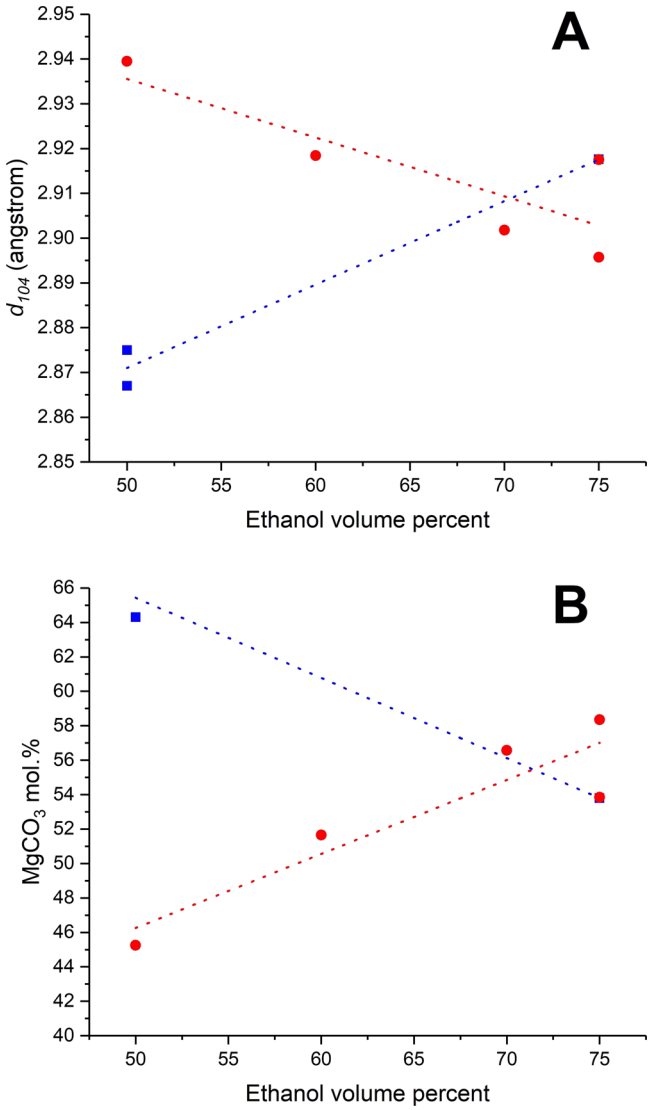

Figure 5. XRD Rietveld refinement results for experiments with 50 mM [Mg^{2+}] at 50 °C as (A) d_{104} value and (B) $MgCO_3$ mol % as a function of ethanol vol %. Red circles correspond to seedless experiments, and blue squares correspond to seeded experiments. Errors associated with the *y*-axes are ±0.004 Å (A) and ±2 mol % (B).

TEM confirmed that smaller crystals in seeded experiments are about ∼100 nm in size, which is consistent with Rietveld refinement results (Figure 7). TEM images did not show convincing evidence of the presence of oriented attachment. HRTEM images and SAED revealed the presence of heterogeneous nucleation of disordered dolomite on calcite (Figure 7). Based on SAED, overgrown disordered dolomite showed a 60° rotation parallel to *a*-axis intergrowth with the underlain calcite seed (Figures 7 and 8).

DISCUSSION

Homogeneous Nucleation in Seedless Experiments from Solutions with Lower Dielectric Constants. We were able to successfully precipitate dolomite precursor phases (HMC and disordered dolomite) in the laboratory at low temperatures using ethanol to remove the hydration barrier around Mg^{2+} that historically has inhibited dolomite precipitation in otherwise dolomite-saturated and thermodynamically favorable conditions.[21,23,25−28] XRD results confirmed the precipitation of disordered dolomite and HMC in our ethanol-added experiments without calcite seeds. Rather than producing perfect dolomite crystals, Ca−Mg carbonates from low-temperature precipitation formed disordered dolomite,[40] likely due to insufficient thermal energy needed to rearrange cations within the crystals. This was evidenced by the absence of *b*-reflections or ordering in cations consistent with other low-temperature Ca−Mg carbonate syntheses[33−38] and computational simulations.[40] For lower-ethanol-concentration experiments, disordered dolomite possessed larger d_{104} values, up to 2.9360 Å, than stoichiometric dolomite (∼2.8978 Å), indicating excess Ca incorporation and disorder in cation sites still partially inhibited by the hydration barrier. In contrast, higher-ethanol experiments showed values close to ideal d_{104} values (∼2.8978 Å) corresponding to $MgCO_3$ mol % of 44 to ∼63%. This indicated that with a much dampened hydration barrier, disordered dolomite could be synthesized from 50 °C

https://doi.org/10.1021/acsomega.1c04624
ACS Omega 2022, 7, 281−292

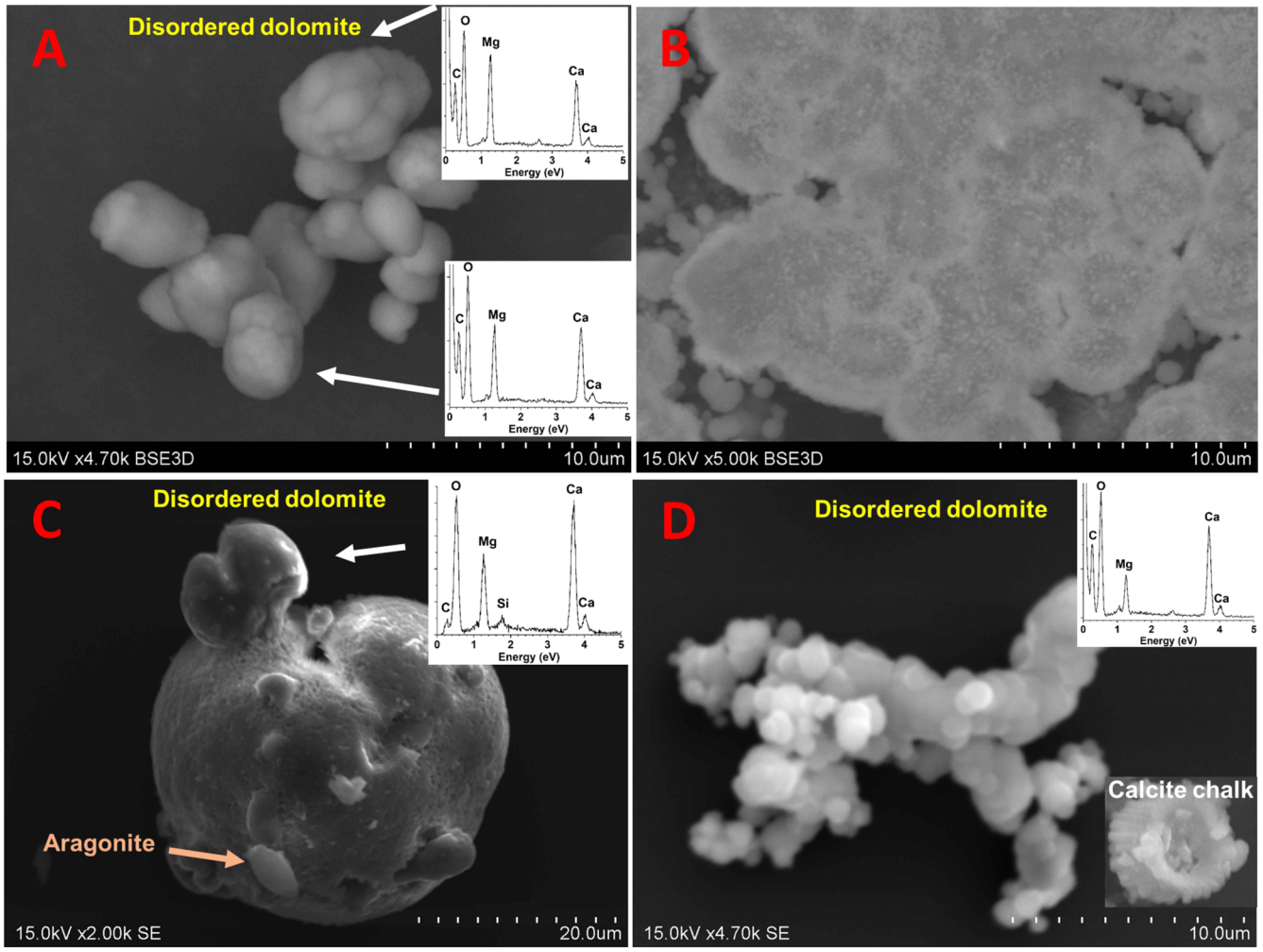

Figure 6. Backscattered electron (BSE; A&B) and secondary electron (SE; C&D) images of synthesized disordered dolomite from 50 vol % ethanol solutions with $[Mg^{2+}]$ = 50 mM and $[Ca^{2+}]$ = 10 mM. Dolomite morphologies formed (A−C) as spherulites without calcite seeds at 25 °C vs (D) as subhedral shapes overgrown on calcite seeds at 50 °C. The inset in lower right in (D) is original calcite chalk (seeds). EDS spectrum from (D) is from disordered dolomite and calcite seed.

to room temperature. Previous work shows a significantly lower Mg incorporation[44] compared to our results which might be the effect of the slow diffusion of ammonium carbonate in their study compared to the predissolved sodium bicarbonate used in this study.

Our data suggest that the ability to promote dehydration, homogeneous nucleation, and Mg incorporation into carbonates from increasing the ethanol content in solutions may stem from the lower dielectric constant of ethanol compared to that of water. Homogeneous nucleation in this study follows the classical nucleation theory that precipitates nucleate in bulk solution and not on substrate surfaces, which did not exclude the formation of amorphous and transient crystalline phases.[51] Using the Born equation (eq 1),[52] we see a clear relationship between the dielectric constant, solvation energy (hydrogen bond and van der Waals bond energies), dehydration (or hydration energy defined as the solvation energy of a solute bonding with water), and Gibbs free energy.

$$\Delta G = -\frac{N_A z^2 e^2}{8\pi\varepsilon_0 r_0}\left(1 - \frac{1}{\varepsilon_r}\right) \quad (1)$$

where N_A is the Avogadro's constant, z is the charge of the ion, e is the elementary charge, ε_0 is the permittivity of free space, r_0 is the effective radius of the ion, and ε_r is the relative permittivity or dielectric constant. Since our synthesis experiments were conducted under similar conditions and the only variable that changed was ε_r, we can simplify eq 1 to

$$|\Delta G| \propto \varepsilon_r \quad (2)$$

This implies that a larger dielectric constant corresponds to a larger solvation energy or dehydration energy. Also solvation energies of cations ($\Delta G^{O}_{s,M^{n+}}$) can be calculated based on the Born equation[53]

$$\Delta G^{O}_{s,M^{n+}} = \omega_{M^{n+}}\left(\frac{1}{\varepsilon} - 1\right) \quad (3)$$

where $\omega_{M^{n+}}$ is the Born solvation coefficient. In the context for this study, the equation will become

$$\Delta G^{O}_{s,Mg^{n+}} = \omega_{Mg^{2+}}\left(\frac{1}{\varepsilon_r} - 1\right) \quad (4)$$

Water has a significantly larger dielectric constant (80.10 at 20 °C) than ethanol[54] (25.10 at 20 °C), and this difference has

https://doi.org/10.1021/acsomega.1c04624
ACS Omega 2022, 7, 281−292

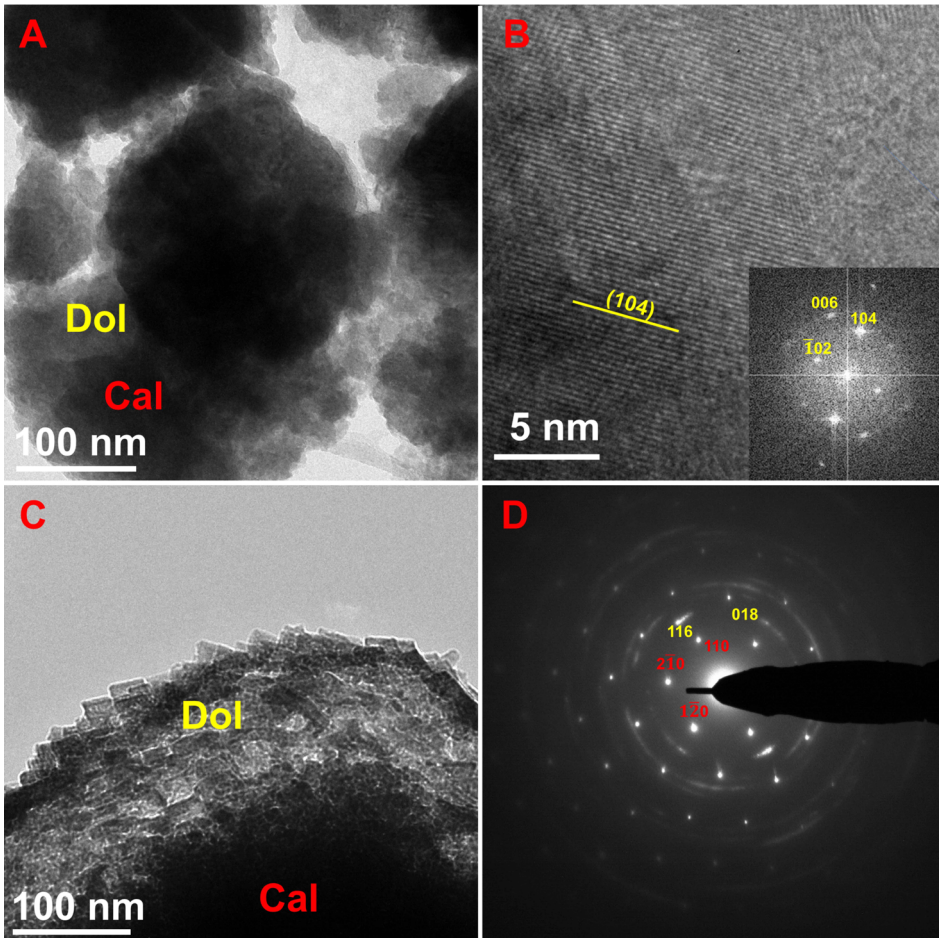

Figure 7. TEM images of synthetic disordered dolomite from 50 vol % ethanol with calcite seeds at 25 °C (A&B) and 50 °C (C). (B) HRTEM image and fast Fourier transform show only the "*a*"-reflection. (D) SAED of disordered dolomite on calcite seed in (C). Red miller indices for calcite seed and yellow for disordered dolomite. Dol = disordered dolomite and Cal = calcite.

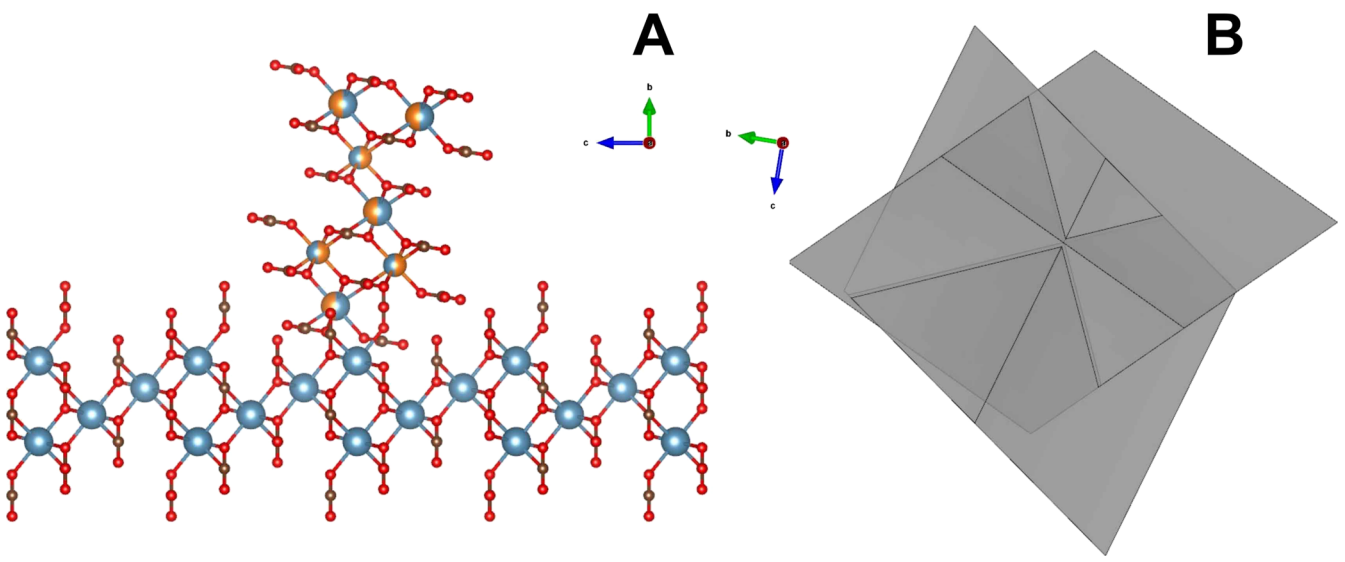

Figure 8. Atomic model of disordered dolomite intergrowth with calcite parallel to the *a*-axis with a 60° rotation. (A) Ball and stick model with calcite on the bottom and disordered dolomite on top. Blue = calcium, orange = magnesium, brown = carbon, and red = oxygen. (B) {104} forms of disordered dolomite and calcite with the same orientation as (A).

been used in the past to create experiments with linearly increasing dielectric constants via water−ethanol mixtures.[55] In our case, dielectric constants of 50 to 75 vol % ethanol solutions decreased from 52.60 to 38.85 at 25 °C. In the meantime, the solvation energy of Mg^{2+} changes from −145.84 (kcal/mol) in pure water to −144.87 (kcal/mol) in 50 vol %

https://doi.org/10.1021/acsomega.1c04624
ACS Omega 2022, 7, 281−292

ethanol solutions to −143.88 (kcal/mol) in 75 vol % ethanol solutions. The decrease in the dielectric constant and solvation energy displayed a linear correlation with mol % $MgCO_3$ in the carbonate precipitates (Figure 9). This strong linear relationship suggests that Mg incorporation in carbonates may be partially controlled by the dielectric constant of the bulk solution and a lower dehydration energy barrier. Previous molecular dynamic (MD) calculation on the catalytic effect of polysaccharides on promoting the Mg−water complex dehydration and disordered dolomite growth demonstrated that a 0.7−1.1 kcal/mol reduction in energy barrier solvation energy is sufficient (Shen et al., 2015). Therefore, the ∼1−2 kcal/mol decrease in solvation energy between ethanol-free solution and 50 vol % ethanol−water mixture and 75 vol % ethanol−water mixture from the decreasing dielectric constant in this study is adequate for disordered dolomite formation. The dehydration energy of calcium will also be affected by the decreased dielectric constant in the solvent. On the other hand, a significantly slower water-exchange rate of Mg^{2+} compared to that of Ca^{2+} resulted in a more stable hydration shell around Mg^{2+}.[32] Increasing ethanol percentage in the solvent might also enhance the Mg^{2+}−solvent exchange and thereafter reduce the stability of the Mg−water complex. Future MD calculations will be needed to understand the exact water change rate increase with increased ethanol and other solvents. The disruption of the Mg−water complex from ethanol also resulted in the decreasing amount of hydromagnesite with increasing ethanol percentage. Nevertheless, Ca is likely to be coordinated more with anions than the solvent as a dissociated ion pair in a lower dielectric constant system based on calcium oxalate experiments.[56] These cation−anion ion pairs in the low-dielectric-constant solvent suggest another potential mechanism for the disruption of the Mg hydration shell in the ethanol solution. It is to be recognized that ethanol has a lower solubility for calcium and magnesium compared to solvents such as water. By replacing a significant portion of water with ethanol, the relative saturation state will increase. Gomaa[57] shows that the calcite solubility product decreases by 1 log unit with every ∼25 mol % increase of ethanol solution. However, increases in the saturation state along could not drive the formation of Ca−Mg carbonate, which has been demonstrated by Land.[4] A recent work demonstrated that magnesite could precipitate under low water activity but not in the bulk solution.[58] Theoretical calculation using MD and metadynamics (MetaD) revealed that certain anions and solvent molecules could facilitate the dehydration of the Mg^{2+}−water complex and foster precipitation of high Mg−carbonate phases.[59] Our experimental data support this calculation result with ethanol affecting the Mg hydration shell and enhance the dehydration of the Mg^{2+}−water complex. Previous studies observed a precipitation shift toward aragonite at a higher ethanol percentage[41,42] which could be a result of faster precipitation as the dehydration energy of calcium decreased. Future studies should investigate this relationship in more detail.

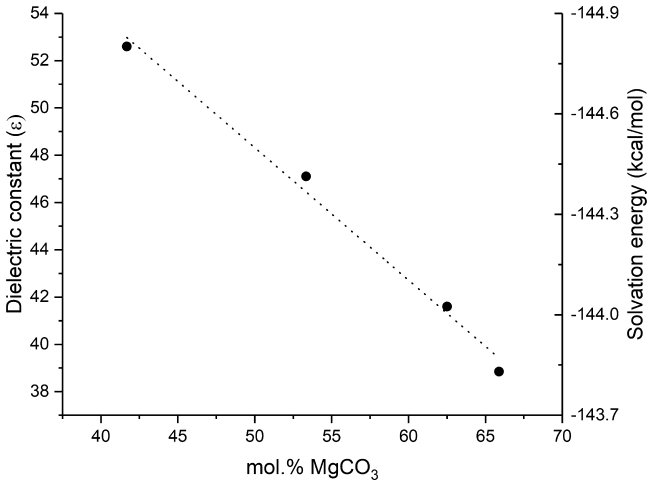

Figure 9. Dielectric constant of the water−ethanol mixture (left) and solvation energy of Mg (right) vs mol % $MgCO_3$ in the precipitated carbonates from seedless experiments. Linear fit for the dielectric constant: $y = -0.56x + 76.34$ and $R^2 = 0.99$.

Heterogeneous Nucleation in Calcite-Seeded Experiments Enhanced by Adsorbed Ethanol Layers. Calcite-seeded experiments show a different pattern for Mg-rich calcium carbonate formation controlled by heterogeneous nucleation. Heterogeneous nucleation of Ca−Mg carbonate on calcite surfaces minimizes the overall energy by reducing the energy-unfavorable solution−crystal interface.[60] The $MgCO_3$ content in precipitated carbonate shows a decreasing trend with increasing ethanol volume percentage, opposite to unseeded experiments (Figures 4 and 5). We suggest that this is because the calcite seeds take up Mg^{2+} at the early stages of dolomite formation, reducing the available Mg in the solution for the new dolomite precipitates to incorporate as they grow. Thus, d_{104} values for the calcite seeds and the precipitated dolomite become more similar over time as the dolomite becomes less Mg-rich (Figure 5).

Calcite surfaces provide heterogeneous nucleation sites in these ethanol−water mixtures that are different compared to simple calcite−water interfaces. Atomic force microscopy and MD simulation studies showed that ethanol layers will preferentially adsorb onto calcite {104} surfaces.[61−64] The adsorbed ethanol will form a ∼6 Å ordered layer and a thicker disordered layer with a gap separating the two ethanol layers.[63] This adsorbed layer creates a hydrophobic layer with $-CH_3$ ends pointing away from the crystal surface.[64−66] These surface-adsorbed layers of alcohol (ethanol, methanol, isopropanol, pentanol, or octanoic acid) bond more strongly with the calcite surface than with water[61,62,67] and inhibit the cation-exchange rate at crystal surfaces to reduce precipitation and dissolution rates for calcite.[64] Inhibition effects from ethanol layers may also lead to decreasing particle sizes with increasing ethanol volume percent.[41] In contrast, ordered surface ethanol layers disrupted at calcite surface steps allow for faster cation exchange, resulting in faster crystal precipitation and dissolution.[64] Because disordered dolomite and HMC precipitated in this study are in the nanometer scale with a high density of step edges, the inhibition effect from surface ethanol layers is likely reduced in our synthesis.

We propose that hydrophobic ethanol layers adsorbed on carbonate surfaces further assisted the dehydration of the Mg−water complex and promoted Mg incorporation. Although previous works have suggested that surface-stable ethanol layers would decelerate calcite growth,[64,67] the hydrophobic ends of the ethanol layer could replace surface water, which would increase the chance for carbonate groups to bond with surface Mg. The calcite seeds in the ethanol−water mixture experiments also further inhibited the formation of aragonite in a Mg-rich solution. This shift in mineralogy compared to the

https://doi.org/10.1021/acsomega.1c04624
ACS Omega 2022, 7, 281−292

control experiments and seedless experiments points to the surface hydrophobic layer enhancing heterogeneous nucleation on calcite surfaces, supplementing the homogeneous nucleation from the reduced dielectric constant of ethanol.

Increased alkalinity in the solutions also had a pronounced effect on promoting Mg incorporation into the calcite structure (Table 2). A higher alkalinity offers higher likelihood for CO_3^{2-} groups to bond with crystal-surface Mg^{2+}. Previous works have also noted an increasing dolomitization rate with higher alkalinity in all experiments.[68−70]

Lattice mismatches with the calcite seeds from a 60° overgrowth rotation, compositional variations, and disordering in cations may have caused thermodynamic instability and inhibited the disordered dolomite crystals from growing into larger crystals. The small size of disordered dolomite crystals was similar to other successful room-temperature synthesis attempts,[34−38,71] and our spherulitic- or irregular-shaped crystal morphologies were similar to other high-ethanol volume % calcite synthesis studies.[41,42] To explain the subhedral dolomite crystals formed in lower-ethanol solutions (30−50 vol %), we propose that the increased availability of water to bond with Mg in low-ethanol solutions could have further inhibited the crystal growth size and led to subhedral crystal shapes. This effect is most noticeable in calcite-seeded experiments (Figure 6). The lower pH in seeded experiments compared to that in seedless experiments is likely due to the increased amount of carbonate from heterogeneous nucleation and changing equilibrium with the additional calcite.

Implication for Ca−Mg Carbonates in Biomineral Systems. Here, we use ethanol as a low-dielectric-constant compound to pave the way for Mg^{2+} to bond with carbonate. Although ethanol is hydrophilic, its polarity and amphipathic nature resulted in a water-repelling hydrophobic layer on the carbonate surface, promoting Mg incorporation. We suggest that this relationship may be an analogue for biomineralization by protein and polysaccharide catalysts that similarly are polar hydrophilic and more importantly amphipathic can create a hydrophobic layer on carbonate surfaces. For example, scleractinian coral CARP3 proteins and soft-bodied coral sclerite-forming proteins, known to help induce Mg-rich calcite formation, are composed of approximately 50% "very hydrophilic" amino acids and less than 10% "very hydrophobic" amino acids.[72−74] HMC is also formed on the exoskeletons of leaf-cutter ants, which are also abundant in chitin and polar hydrophilic and amphipathic amino acids.[75] HMC and disordered dolomite precipitated by crustose coralline algae are likely induced by polysaccharides which are polar, hydrophilic, and amphipathic such as carrageenan.[76−79]

CONCLUSIONS

Disordered dolomite and high Mg-calcite can directly precipitate through homogeneous nucleation at room temperature by lowering the dielectric constant of the solution, with a linear relationship between a decreasing solution dielectric constant and increasing Mg incorporation. In scenarios of heterogeneous nucleation on calcite seeds, adsorbed hydrophobic surface layers help to further promote Mg incorporation in Mg-rich calcium carbonate precipitates. Although high-ethanol-percentage solutions do not exist in natural environments, this work provides a detailed understanding of the formation of Ca−Mg carbonates and Mg incorporation into carbonates by testing the chemical properties at play (ex: dielectric constant, alkalinity, polarity, and hydrophobicity). The hydrophobic effect of surface ethanol layers and the polarity of ethanol also provide a possible mechanism for Ca−Mg carbonate precipitation in biomineralizing organisms. For instance, polysaccharides such as carrageenans and amino acids such as aspartic acids and glutamic acids could be responsible for precipitating Mg-rich carbonates.

ASSOCIATED CONTENT

Supporting Information

The Supporting Information is available free of charge at https://pubs.acs.org/doi/10.1021/acsomega.1c04624.

Representative XRD Rietveld refinement results from synthesis experiments with and without calcite seeds and mineral assemblages for synthesis experiments based on XRD Rietveld refinement (PDF)

AUTHOR INFORMATION

Corresponding Author

Huifang Xu − *NASA Astrobiology Institute, Department of Geoscience, University of Wisconsin−Madison, Madison, Wisconsin 53706, United States;* orcid.org/0000-0002-7464-0057; Email: hfxu@geology.wisc.edu

Authors

Yihang Fang − *NASA Astrobiology Institute, Department of Geoscience, University of Wisconsin−Madison, Madison, Wisconsin 53706, United States; Department of Mineral Sciences, National Museum of Natural History, Smithsonian Institution, Washington, District of Columbia 20560, United States;* orcid.org/0000-0002-8218-5883

Fangfu Zhang − *NASA Astrobiology Institute, Department of Geoscience, University of Wisconsin−Madison, Madison, Wisconsin 53706, United States*

Gabriela A. Farfan − *Department of Mineral Sciences, National Museum of Natural History, Smithsonian Institution, Washington, District of Columbia 20560, United States*

Complete contact information is available at: https://pubs.acs.org/10.1021/acsomega.1c04624

Notes

The authors declare no competing financial interest.

ACKNOWLEDGMENTS

We would like to thank Dr. Deqing Zhang for handling our manuscript and the two anonymous reviewers for their constructive suggestions. This work was supported by the NASA Astrobiology Institute (NNA 13AA94A), S.W. Bailey Fellowship of the Department of Geoscience, University of Wisconsin−Madison, and the Big 10 Academic Alliance Smithsonian Institution Fellowship.

REFERENCES

(1) Van Tuyl, F. M. The Origin of Dolomite. *Iowa Geol. Surv., Annu. Rep.* **1914**, *XXV*, 251−421.

(2) Zengler, D. H.; Dunham, J. D.; Ethington, R. L. Concepts and Models of Dolomitization. *Spec. Publ.—SEPM* **1980**, *No. 28*, 320.

(3) Tucker, M. E.; Wright, V. P. *Carbonate Sedimentology*; Blackwell Publishing: Malden, MA, 1990.

(4) Land, L. S. Failure to Precipitate Dolomite at 25°C from Dilute Solution despite 1000-Fold Oversaturation after 32 Years. *Aquat. Geochem.* **1998**, *4*, 361−368.

(5) Kaczmarek, S. E.; Gregg, J. M.; Bish, D. L.; Machel, H. G.; Fouke, B. W.; Fouke, B. W.; Fouke, B. W.; Gregg, J. M.; Bish, D. L.; Machel, H. G.; et al. Dolomite, Very High-magnesium Calcite, and Microbes-implications for the Microbial Model of Dolomitization. *SEPM Spec. Publ.* **2017**, *109*, 1−14.
(6) Petrash, D. A.; Bialik, O. M.; Bontognali, T. R. R.; Vasconcelos, C.; Roberts, J. A.; McKenzie, J. A.; Konhauser, K. O. Microbially Catalyzed Dolomite Formation: From near-Surface to Burial. *Earth-Sci. Rev.* **2017**, *171*, 558−582.
(7) Rosen, M. R.; Miser, D. E.; Warren, J. K. Sedimentology, Mineralogy and Isotopic Analysis of Pellet Lake, Coorong Region, South Australia. *Sedimentology* **1988**, *35*, 105−122.
(8) Last, W. M. Lacustrine Dolomite-an Overview of Modern, Holocene, and Pleistocene Occurrences. *Earth-Sci. Rev* **1990**, *27*, 221−263.
(9) Peterson, M. N. A.; Bien, G. S.; Berner, R. A. Radiocarbon studies of recent dolomite from Deep Spring Lake, California. *J. Geophys. Res.* **1963**, *68*, 6493−6505.
(10) Lumsden, D. N. Characteristics of Deep-Marine Dolomite. *J. Sediment. Res.* **1988**, *58*, 1023−1031.
(11) Gregg, J. M.; Frank, T. D. Data Report : Dolomite in Neogene Sediments of the Belgica Carbonate Mound Province , Porcupine Seabight , North Atlantic 1. *Proc. Integr. Ocean Drill. Progr.* **2009**, *307*, 1−12.
(12) Lu, Y.; Sun, X.; Xu, H.; Konishi, H.; Lin, Z.; Xu, L.; Chen, T.; Hao, X.; Lu, H.; Peckmann, J. Formation of dolomite catalyzed by sulfate-driven anaerobic oxidation of methane: Mineralogical and geochemical evidence from the northern South China Sea. *Am. Mineral.* **2018**, *103*, 720−734.
(13) Xu, H. Synergistic Roles of Microorganisms in Mineral Precipitates Associated with Deep Sea Methane Seeps. In *Geomicrobiology: Molecular and Environmental Perspective2*; Springer, 2010; pp 325−346.
(14) Vasconcelos, C.; McKenzie, J. A. Microbial Mediation of Modern Dolomite Precipitation and Diagenesis under Anoxic Conditions (Lagoa Vermelha, Rio de Janeiro, Brazil). *J. Sediment. Res.* **1997**, *67*, 378−390.
(15) Curtis, R.; Evans, G.; Kinsman, D. J. J.; Shearman, D. J. Association of Dolomite and Anhydrite in the Recent Sediments of the Persian Gulf. *Nature* **1963**, *197*, 679−680.
(16) Kendall, G. S. C.; Skipwith, P. A. d'E. Recent Algal Mats of a Persian Gulf Lagoon. *J. Sediment. Res.* **1968**, *38*, 1040−1058.
(17) Meister, P.; Mckenzie, J. A.; Vasconcelos, C.; Bernasconi, S.; Frank, M.; Gutjahr, M.; Schrag, D. P. Dolomite formation in the dynamic deep biosphere: results from the Peru Margin. *Sedimentology* **2007**, *54*, 1007−1032.
(18) Deelman, J. C.; Gidman, J.; Gaines, A. M. Protodolomite redefined; discussion and reply. *J. Sediment. Petrol.* **1978**, *48*, 1004−1011.
(19) Goldsmith, J. R.; Heard, H. C. Subsolidus Phase Relations in the System $CaCO_3$-$MgCO_3$. *J. Geol.* **1961**, *69*, 45−74.
(20) Goldsmith, J. R.; Graf, D. L. Structural and Compositional Variations in Some Natural Dolomites. *J. Geol.* **1958**, *66*, 678−693.
(21) Lippmann, F. The Polymorphism Calcite-Aragonite. In *Sedimentary Carbonate Minerals*; Springer: New York, 1973.
(22) Noyes, R. M. Thermodynamics of Ion Hydration as a Measure of Effective Dielectric Properties of Water. *J. Am. Chem. Soc.* **1962**, *84*, 513−522.
(23) Raz, S.; Weiner, S.; Addadi, L. Formation of High-Magnesian Calcites via an Amorphous Precursor Phase: Possible Biological Implications. *Adv. Mater.* **2000**, *12*, 38−42.
(24) Gautier, Q.; Bénézeth, P.; Mavromatis, V.; Schott, J. Hydromagnesite solubility product and growth kinetics in aqueous solution from 25 to 75°C. *Geochim. Cosmochim. Acta* **2014**, *138*, 1−20.
(25) Mucci, A.; Morse, J. W. The Incorporation of Mg^{2+} and Sr^{2+} into Calcite Overgrowths: Influences of Growth Rate and Solution Composition. *Geochim. Cosmochim. Acta* **1983**, *47*, 217−233.
(26) Astilleros, J. M.; Fernandez-Diaz, L.; Putnis, A. The Role of Magnesium in the Growth of Calcite: An AFM Study. *Chem. Geol.* **2010**, *271*, 52−58.
(27) de Leeuw, N. H.; Parker, S. C. Surface-Water Interactions in the Dolomite Problem. *Phys. Chem. Chem. Phys.* **2001**, *3*, 3217−3221.
(28) Higgins, S. R.; Hu, X. Self-Limiting Growth on Dolomite: Experimental Observations with in Situ Atomic Force Microscopy. *Geochim. Cosmochim. Acta* **2005**, *69*, 2085−2094.
(29) Shen, Z.; Liu, Y.; Brown, P. E.; Szlufarska, I.; Xu, H. Modeling the Effect of Dissolved Hydrogen Sulfide on Mg^{2+}−Water Complex on Dolomite {104} Surfaces. *J. Phys. Chem. C* **2014**, *118*, 15716.
(30) Konigsberger, E.; Konigsberger, L.-C.; Gamsjager, H. Low Temperature Thermodynamic Model for the System Na_2CO_3-$MgCO_3$-$CaCO_3$-H_2O. *Geochim. Cosmochim. Acta* **1999**, *63*, 3105−3119.
(31) Fischbeck, R.; Müller, G. Monohydrocalcite, Hydromagnesite, Nesquehonite, Dolomite, Aragonite, and Calcite in Speleothems of the Fränkische Schweiz, Western Germany. *Contrib. Mineral. Petrol.* **1971**, *33*, 87−92.
(32) Xu, J.; Yan, C.; Zhang, F.; Konishi, H.; Xu, H.; Teng, H. H. Testing the cation-hydration effect on the crystallization of Ca-Mg-CO_3 systems. *Proc. Natl. Acad. Sci. U.S.A.* **2013**, *110*, 17750−17755.
(33) Oomori, T.; Kitano, Y. Synthesis of Protodolomite from Sea Water Containing Dioxane. *Geochem. J.* **1987**, *21*, 59−65.
(34) Zhang, F.; Xu, H.; Konishi, H.; Kemp, J. M.; Roden, E. E.; Shen, Z. Dissolved Sulfide-Catalyzed Precipitation of Disordered Dolomite: Implications for the Formation Mechanism of Sedimentary Dolomite. *Geochim. Cosmochim. Acta* **2012**, *97*, 148−165.
(35) Zhang, F.; Xu, H.; Konishi, H.; Shelobolina, E. S.; Roden, E. E. Polysaccharide-Catalyzed Nucleation and Growth of Disordered Dolomite: A Potential Precursor of Sedimentary Dolomite. *Am. Mineral.* **2012**, *97*, 556−567.
(36) Zhang, F.; Xu, H.; Shelobolina, E. S.; Konishi, H.; Converse, B.; Shen, Z.; Roden, E. E. The Catalytic Effect of Bound Extracellular Polymeric Substances Excreted by Anaerobic Microorganisms on Ca-Mg Carbonate Precipitation: Implications for the "Dolomite Problem. *Am. Mineral.* **2015**, *100*, 483−494.
(37) Hobbs, F. W. C.; Xu, H. Magnesite Formation through Temperature and pH Cycling as a Proxy for Lagoon and Playa Paleoenvironments. *Geochim. Cosmochim. Acta* **2020**, *269*, 101.
(38) Fang, Y.; Xu, H. Dissolved Silica-Catalyzed Disordered Dolomite Precipitation. *Am. Mineral.* **2022**, *107*, in press. DOI: 10.2138/am-2021-7474.
(39) Pimentel, C.; Pina, C. M. Reaction Pathways towards the Formation of Dolomite-Analogues at Ambient Conditions. *Geochim. Cosmochim. Acta* **2016**, *178*, 259−267.
(40) Bruno, M.; Ghignone, S.; Pastero, L.; Aquilano, D. The Influence of Ca-Mg Disorder on the Growth of Dolomite: A Computational Study. *CrystEngComm* **2020**, *22*, 4853−4861.
(41) Seo, K. S.; Han, C.; Wee, J. H.; Park, J. K.; Ahn, J. W. Synthesis of Calcium Carbonate in a Pure Ethanol and Aqueous Ethanol Solution as the Solvent. *J. Cryst. Growth* **2005**, *276*, 680−687.
(42) Sand, K. K.; Rodriguez-Blanco, J. D.; Makovicky, E.; Benning, L. G.; Stipp, S. L. S. Crystallization of $CaCO_3$ in Water-Alcohol Mixtures: Spherulitic Growth, Polymorph Stabilization, and Morphology Change. *Cryst. Growth Des.* **2012**, *12*, 842−853.
(43) Liu, Y.-Y.; Jiang, J.; Gao, M.-R.; Yu, B.; Mao, L.-B.; Yu, S.-H. Phase Transformation of Magnesium Amorphous Calcium Carbonate (Mg-ACC) in a Binary Solution of Ethanol and Water. *Cryst. Growth Des.* **2013**, *13*, 59−65.
(44) Falini, G.; Gazzano, M.; Ripamonti, A. Magnesium calcite crystallizatin from water-alcohol mixtures. *Chem. Commun.* **1996**, *9*, 1037−1038.
(45) Gregg, J. M.; Bish, D. L.; Kaczmarek, S. E.; Machel, H. G. Mineralogy, Nucleation and Growth of Dolomite in the Laboratory and Sedimentary Environment: A Review. *Sedimentology* **2015**, *62*, 1749−1769.

https://doi.org/10.1021/acsomega.1c04624
ACS Omega 2022, 7, 281−292

(46) Fang, Y.; Xu, H. A New Approach To Quantify the Ordering State of Protodolomite Using XRD, TEM, and Z-Contrast Imaging. *J. Sediment. Res.* **2019**, *89*, 537−551.
(47) Kaczmarek, S. E.; Thornton, B. P. The Effect of Temperature on Stoichiometry, Cation Ordering, and Reaction Rate in High-Temperature Dolomitization Experiments. *Chem. Geol.* **2017**, *468*, 32−41.
(48) Parkhurst, D. L.; Appelo, C. A. J. *Description of Input and Examples for PHREEQC Version 3−A Computer Program for Speciation, Batch-Reaction, One-Dimensional Transport, and Inverse Geochemical Calculations*; U.S. Geological Survey. 2013.
(49) Zhang, F.; Xu, H.; Konishi, H.; Roden, E. E. A Relationship between d_{104} Value and Composition in the Calcite-Disordered Dolomite Solid-Solution Series. *Am. Mineral.* **2010**, *95*, 1650−1656.
(50) Montes-Hernandez, G.; Renard, F.; Auzende, A.-L.; Findling, N. Amorphous Calcium-Magnesium Carbonate (ACMC) Accelerates Dolomitization at Room Temperature under Abiotic Conditions. *Cryst. Growth Des.* **2020**, *20*, 1434−1441.
(51) Oxtoby, D. W. Homogeneous Nucleation: Theory and Experiment. *J. Phys. Condens. Matter* **1992**, *4*, 7627−7650.
(52) Atkins, P. W.; MacDermott, A. J. The Born Equation and Ionic Solvation. *J. Chem. Educ.* **1982**, *59*, 359−360.
(53) Xu, H.; Xu, D. C.; Wang, Y. Natural Indices for the Chemical Hardness/Softness of Metal Cations and Ligands. *ACS Omega* **2017**, *2*, 7185−7193.
(54) Mohsen-Nia, M.; Amiri, H.; Jazi, B. Dielectric Constants of Water, Methanol, Ethanol, Butanol and Acetone: Measurement and Computational Study. *J. Solution Chem.* **2010**, *39*, 701−708.
(55) Wyman, J. J. The Dielectric Constant of Mixtures of Ethyl Alcohol and Water from -5 to 40. *J. Am. Chem. Soc.* **1931**, *539*, 3293−3301.
(56) Molzon, J. A.; Lausier, J. M.; Paruta, A. N. Solubility of Calcium Oxalate in 1-alkanols and Ethanol-Water Mixtures. *J. Pharm. Sci.* **1978**, *67*, 733−735.
(57) Gomaa, E. A. Solubility and Solvation Parameters of Calcium Carbonate in Mixed Ethanol-Water Mixtures at 301.15 K. *Sci. Technol.* **2012**, *2*, 51−52.
(58) Mergelsberg, S. T.; Kerisit, S. N.; Ilton, E. S.; Qafoku, O.; Thompson, C. J.; Loring, J. S. Low Temperature and Limited Water Activity Reveal a Pathway to Magnesiteviaamorphous Magnesium Carbonate. *Chem. Commun.* **2020**, *56*, 12154−12157.
(59) Toroz, D.; Song, F.; Chass, G. A.; Di Tommaso, D. New Insights into the Role of Solution Additive Anions in Mg^{2+} Dehydration: Implications for Mineral Carbonation. *CrystEngComm* **2021**, *23*, 4896−4900.
(60) Giuffre, A. J.; Hamm, L. M.; Han, N.; De Yoreo, J. J.; Dove, P. M. Polysaccharide Chemistry Regulates Kinetics of Calcite Nucleation through Competition of Interfacial Energies. *Proc. Natl. Acad. Sci. U.S.A.* **2013**, *110*, 9261−9266.
(61) Cooke, D. J.; Gray, R. J.; Sand, K. K.; Stipp, S. L. S.; Elliott, J. A. Interaction of Ethanol and Water with the {10$\bar{1}$4} Surface of Calcite. *Langmuir* **2010**, *26*, 14520−14529.
(62) Sand, K. K.; Yang, M.; Makovicky, E.; Cooke, D. J.; Hassenkam, T.; Bechgaard, K.; Stipp, S. L. S. Binding of Ethanol on Calcite: The Role of the OH Bond and Its Relevance to Biomineralization. *Langmuir* **2010**, *26*, 15239−15247.
(63) Pasarín, I. S.; Yang, M.; Bovet, N.; Glyvradal, M.; Nielsen, M. M.; Bohr, J.; Feidenhansâ, R.; Stipp, S. L. S. Molecular Ordering of Ethanol at the Calcite Surface. *Langmuir* **2011**, *28*, 2545−2550.
(64) Keller, K. S.; Olsson, M. H. M.; Yang, M.; Stipp, S. L. S. Adsorption of Ethanol and Water on Calcite: Dependence on Surface Geometry and Effect on Surface Behavior. *Langmuir* **2015**, *31*, 3847−3853.
(65) Pasarín, I. S.; Bovet, N.; Glyvradal, M.; Nielsen, M. M.; Bohr, J.; Feidenhansl, R.; Stipp, S. L. S. Atomic Modifications by Synchrotron Radiation at the Calcite-Ethanol Interface. *J. Synchrotron Radiat.* **2012**, *19*, 530−535.
(66) Bovet, N.; Yang, M.; Javadi, M. S.; Stipp, S. L. S. Interaction of Alcohols with the Calcite Surface. *Phys. Chem. Chem. Phys.* **2013**, *17*, 3490.
(67) Hakim, S. S.; Olsson, M. H. M.; Sørensen, H. O.; Bovet, N.; Bohr, J.; Feidenhans'l, R.; Stipp, S. L. S. Interactions of the Calcite {10.4} Surface with Organic Compounds: Structure and Behaviour at Mineral - Organic Interfaces. *Sci. Rep.* **2017**, *7*, 7592−11.
(68) Morrow, D. W.; Ricketts, B. D. Experimental Investigation of Sulfate Inhibition of Dolomite and Its Mineral Analogues. *Sedimentol. Geochem. Dolostones* **1988**, *43*, 25.
(69) Arvidson, R. S.; Mackenzie, F. T. Tentative Kinetic Model for Dolomite Precipitation Rate and Its Application to Dolomite Distribution. *Aquat. Geochem.* **1997**, *2*, 273−298.
(70) Arvidson, R. S.; Mackenzie, F. T. The Dolomite Problem: Control of Precipitation Kinetics by Temperature and Saturation State. *Am. J. Sci.* **1999**, *299*, 257−288.
(71) Zhang, F.; Yan, C.; Teng, H. H.; Roden, E. E.; Xu, H. In Situ AFM Observations of Ca-Mg Carbonate Crystallization Catalyzed by Dissolved Sulfide: Implications for Sedimentary Dolomite Formation. *Geochim. Cosmochim. Acta* **2013**, *105*, 44−55.
(72) Gavriel, R.; Nadav-Tsubery, M.; Glick, Y.; Yarmolenko, A.; Kofman, R.; Keinan-Adamsky, K.; Berman, A.; Mass, T.; Goobes, G. The Coral Protein CARP3 Acts from a Disordered Mineral Surface Film to Divert Aragonite Crystallization in Favor of Mg-Calcite. *Adv. Funct. Mater.* **2018**, *28*, 1707321.
(73) Mass, T.; Drake, J. L.; Haramaty, L.; Kim, J. D.; Zelzion, E.; Bhattacharya, D.; Falkowski, P. G. Cloning and Characterization of Four Novel Coral Acid-Rich Proteins That Precipitate Carbonates in Vitro. *Curr. Biol.* **2013**, *23*, 1126−1131.
(74) Rahman, M. A.; Oomori, T.; Wörheide, G. Calcite Formation in Soft Coral Sclerites Is Determined by a Single Reactive Extracellular Protein. *J. Biol. Chem.* **2011**, *286*, 31638−31649.
(75) Li, H.; Sun, C. Y.; Fang, Y.; Carlson, C. M.; Xu, H.; Ješovnik, A.; Sosa-Calvo, J.; Zarnowski, R.; Bechtel, H. A.; Fournelle, J. H.; et al. Biomineral Armor in Leaf-Cutter Ants. *Nat. Commun.* **2020**, *11*, 5792.
(76) Nash, M. C.; Adey, W.; Harvey, A. S. High Magnesium Calcite and Dolomite Composition Carbonate in Amphiroa (Lithophyllaceae, Corallinales, Rhodophyta): Further Documentation of Elevated Mg in Corallinales with Climate Change Implications. *J. Phycol.* **2021**, *57*, 496−509.
(77) Diaz-Pulido, G.; Nash, M. C.; Anthony, K. R.; Bender, D.; Opdyke, B. N.; Reyes-Nivia, C.; Troitzsch, U. Greenhouse Conditions Induce Mineralogical Changes and Dolomite Accumulation in Coralline Algae on Tropical Reefs. *Nat. Commun.* **2014**, *5*, 3310.
(78) Nash, M. C.; Adey, W. Multiple Phases of Mg-Calcite in Crustose Coralline Algae Suggest Caution for Temperature Proxy and Ocean Acidification Assessment: Lessons from the Ultrastructure and Biomineralization in Phymatolithon (Rhodophyta, Corallinales)1. *J. Phycol.* **2017**, *53*, 970−984.
(79) Martone, P. T.; Navarro, D. A.; Stortz, C. A.; Estevez, J. M. Differences in Polysaccharide Structure between Calcified and Uncalcified Segments in the Coralline Calliarthron Cheilosporioides (Corallinales, Rhodophyta)1. *J. Phycol.* **2010**, *46*, 507−515.

https://doi.org/10.1021/acsomega.1c04624
ACS Omega 2022, 7, 281−292